AN UNSUPERVISED APPROACH TO DETECT MICROGLIA TIP IN VOLUMETRIC FLUORESCENCE IMAGING DATA

Mengfan Wang[⋆] *Kathleen Whiting*[†] *Fritz W. Lischka*[†] *Zygmunt Galdzicki*[†] *Guoqiang Yu*[⋆]

[⋆] Bradley Department of Electrical and Computer Engineering, Virginia Tech, Arlington, VA, USA

[†] Department of Anatomy, Physiology, and Genetics, School of Medicine, Uniformed Services University of the Health Sciences, Bethesda, MD, USA

ABSTRACT

Microglia play a key role in maintaining brain health, and the detection of microglia tips is essential for analyzing their motility. However, current tip detection methods either rely on deep neural networks, which require time-consuming annotations, or are unsupervised methods analyzing local patterns, which are significantly influenced by the microglia morphology change. In this paper, we propose an unsupervised, multi-scale microglia tip detection approach. Our approach measures the distance between the candidate tip and the convex hull of adjacent pixels to eliminate the influence of morphology variation. We demonstrated the new approach on volumetric fluorescence imaging data and achieved superior performance compared to peer algorithms.

***Index Terms*—** Microglia, tip detection, unsupervised learning, fluorescence imaging, volumetric data, convex hull

1. INTRODUCTION

Microglia, a sub-type of the glial family, are macrophage cells located in the brain and spinal cord and play a crucial role as defenders and sculptors of the central nervous system [1]. As the main form of active immune defense in the brain, microglia are responsible for the phagocytosis of pathogens and apoptotic cells as well as modulating adaptive immune response. They have also been identified to be essential for modulating synaptic structure, synaptic physiology, and have recently been implicated in learning and memory processes [2][3][4][5][6].

Mature microglia have multiple highly dynamic processes displaying considerable structural changes and exhibiting distinct morphological transition states when executing certain functions [5]. Therefore, the detection and quantification of processes and tips is a key component of demonstrating microglia activity. However, manual annotation is quite time-consuming, especially when dealing with volumetric data, which causes pure manual labeling to be unrealistic. Besides, the lack of a dataset with ground truth for supervised learning requires vast annotated data, especially for deep neural networks [7] [8].

General unsupervised tip detection methods are developed to distinguish tip regions by local patterns. One type of local pattern is the angle of tip. For example, the ray shooting model was proposed to detect the neuron tip in volumetric images by calculating the angle of rays shooting from tip to foreground [9]. Another method calculates the maximum product of neighbor foreground to detect pixels with the minimum angle for decomposing branches [10]. Curvature is another category of local pattern. Gaussian curvature is used to detect nose tips [11] and the authors in [12] proposed a method based on principal curvature to detect corners, which has been used for plant root tip detection [13].

However, the size and morphology of microglia tips vary significantly during the transition states. This makes general unsupervised tip detection approaches more challenging to extend, although these have been broadly applied in similar tasks utilizing different strategies. In this paper, we propose a novel approach specific to microglia tip detection. Instead of identifying the local pattern, the proposed method focuses on the distance to the adjacent convex hull to eliminate the influence of the changes in microglia morphology. In addition, the method works on multi-scales for improved robustness. Extensive analysis of microglia imaging datasets confirmed the superiority of our proposed approach.

2. METHODS

The proposed method includes three steps: geodesic distance calculation, pixel to convex hull distance calculation, and finding tips from score map. We assume that foreground is already segmented and the model works on the surface pixels, which are foreground pixels that connect with the background.

The first step is to calculate the geodesic distance from every surface pixel to its neighbor foreground pixels and then select pixels with the appropriate distance controlled by a scale s. The selected pixels are called adjacent pixels of the sur-

face pixel. In the second step, we find the distance between the surface pixel and the convex hull of the adjacent pixels shown in Fig. 1. The distance measure has two advantages. On one hand, the distance d is related to the convexity of the local region. The more salient the region is, the more likely it is a tip, and the larger d will be. On the other hand, the distance measure is less affected by the morphology of tips when compared to peer methods. The final score map consists of measurements of all surface pixels under all different scales. Finally, we extract the tips from the 4-dimensional score map.

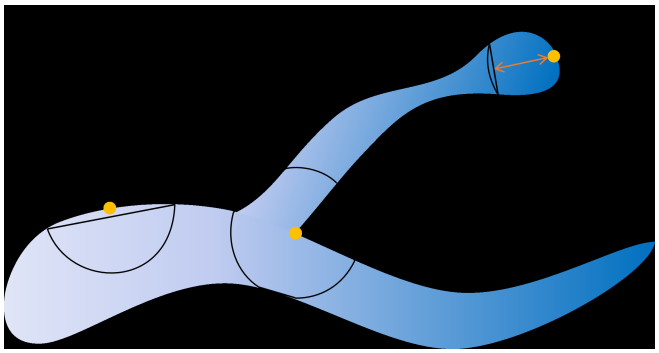

Fig. 1. A branch of microglia with examples of three kinds of surface pixels and convex hulls of their adjacent pixels. The surface pixels are yellow while the convex hulls including adjacent pixels are black. (a) A tip, whose distance to the convex hull d is larger than 0. (b) A ramification in the convex hull and the distance is 0. (c) A pixel on flat region, the distance is close to 0.

2.1. Geodesic distance calculation

For a surface pixel $\mathbf{p} \in \mathbb{F}$, the corresponding adjacent pixels under the scale s is a set

$$Q_{\mathbf{p},s} = \{\mathbf{q} : |d_G(\mathbf{p},\mathbf{q}) - s| \leq \epsilon, \forall \mathbf{q} \in \mathbb{F}\}, \tag{1}$$

where $\mathbb{F} \subset \mathbb{R}^3$ is all foreground pixels, $d_G(\cdot)$ is the geodesic distance measure and ϵ is a small number. Usually, we set $\epsilon = 0.5$.

The distance calculation problem is similar to all pairs of shortest path (APSP) problem, which finds all shortest paths between any two nodes in a graph. In our problem, we only need to calculate the distance from the surface pixel to neighbor foreground pixels. Traditional shortest path algorithms, such as Dijkstra and Floyd-Warshall, can solve the problem in an inefficient way. In fact, any comparison-based shortest-path algorithms are inefficient to our problem because the length of edges has very limited choices, which means many comparisons are unnecessary. A better strategy is grassfire transform [14] in linear time complexity. With slight modification, the total time complexity can be $O(mn)$, where n is the number of surface pixels and m is the number of neighbor foreground pixels under the maximum scale. It worth noting that the geodesic distances only need to be calculated once even though there are multiple scales.

2.2. Pixel to convex hull distance calculation

The convex hull of the adjacent pixels $conv(Q_{\mathbf{p},s})$ is the smallest convex set containing $Q_{\mathbf{p},s}$. We have

$$conv(Q_{\mathbf{p},s}) = \{\sum_i \lambda_i \mathbf{w}_i : \lambda_i \geq 0, \sum_i \lambda_i = 1, \mathbf{w}_i \in Q_{\mathbf{p},s}\} \tag{2}$$

The second step is to calculate the smallest Euclidean distance between the surface pixel and the convex hull

$$d_{\mathbf{p},s} = \min_{\mathbf{q}} ||\mathbf{p} - \mathbf{q}||, \forall \mathbf{q} \in conv(Q_{\mathbf{p},s}) \tag{3}$$

The pixel to convex hull distance calculation is based on the open Gilbert-Johnson-Keerthi (GJK) package [15]. The GJK algorithm [16] is a method of determining the minimum distance between two convex sets by iteratively generating closer simplices to the correct answer, and the open GJK package updated the sub-algorithm in a faster way. We reimplemented the package for two reasons. The most important reason is that the original package is not reliable enough and gives inaccurate results occasionally. What's more, our problem is to find the minimum distance between a point and a convex set, which could be processed more simply.

The time complexity of the GJK algorithm is almost constant and no more than linear [17] so that the total time complexity of the second step is still $O(mn)$.

2.3. Finding tips from score map

The method is proposed to calculate score maps under multiple scales, which are defined as a set $\mathcal{S}$, to detect tips with different sizes. A surface pixel is possible to be a tip even though it gets a high score under one certain scale only. We combine all normalized scores of a surface pixel and get the maximum one:

$$d_{\mathbf{p}}^{max} = \max_s \frac{d_{\mathbf{p},s}}{s}, \forall s \in \mathcal{S} \tag{4}$$

After normalization, $d_{\mathbf{p}}^{max} \in [0,1]$. $d_{\mathbf{p}}^{max}$ may be influenced by the imperfect foreground segmentation result. To eliminate the influence, the final score takes the average of a local region:

$$d_{\mathbf{p}}^{avg} = \frac{1}{N} \sum_{\mathbf{q}} d_{\mathbf{q}}^{max}, d_G(\mathbf{p},\mathbf{q}) \leq \gamma, \tag{5}$$

where N is the number of all $\mathbf{q}$. As a rule of thumb, we set $\gamma = 2$.

If $d_{\mathbf{p}}^{avg}$ is a local maximum of its neighbors:

$$d_{\mathbf{p}}^{avg} = \max_{\mathbf{q}} d_{\mathbf{q}}^{avg}, d_G(\mathbf{p},\mathbf{q}) \leq \gamma, \tag{6}$$

$\mathbf{p}$ is a candidate tip. A higher score represents a larger possibility of being a real tip. $d_{\mathbf{p}}^{max}$ and $d_{\mathbf{p}}^{avg}$ can be found in $O(n)$ time complexity.

Algorithm 1 shows the pseudocode of the whole pipeline. A more detailed analysis is in the supplementary.

Algorithm 1 Tip detection algorithm

Input: Foreground $\mathbb{F}$, distance scale set $\mathcal{S}$, smoothness γ
Output: Tip list with scores $(\mathbf{p}, d)$

for every surface pixel $\mathbf{p}$ **do**
  $Q_{\mathbf{p}} = \text{GrassfireTransform}(\mathbf{p}, \mathbb{F}, \mathcal{S})$
  for $s \in \mathcal{S}$ **do**
    $d_{\mathbf{p},s} = \text{GJK}(\mathbf{p}, Q_{\mathbf{p},s})$
  end for
end for
$d_{\mathbf{p}}^{max} = \max_s \frac{d_{\mathbf{p},s}}{s}, \forall s \in \mathcal{S}, \forall \mathbf{p}$
$d_{\mathbf{p}}^{avg} = \frac{1}{N} \sum_{\mathbf{q}} d_{\mathbf{q}}^{max}, d_G(\mathbf{p}, \mathbf{q}) \leq \gamma, \forall \mathbf{p}$
for every $\mathbf{p}$ **do**
  if $d_{\mathbf{p}}^{avg} = \max_{\mathbf{q}} d_{\mathbf{q}}^{avg}, d_G(\mathbf{p}, \mathbf{q}) \leq \gamma$ **then**
    Output $(\mathbf{p}, d_{\mathbf{p}}^{avg})$
  end if
end for

3. EXPERIMENTS

3.1. Peer methods and data

Few methods are aimed at microglia tip detection, but some methods perform very similar tasks, such as the ray shooting model (RS) [9], branch decomposition (BS) [10], and Gaussian curvature (GC) mentioned in Section 1. In [18], the authors proposed a score, shape index (SI), based on principle curvature to detect tips.

We did the experiment on our imaging data describing the microglia activity in mouse brain after vascular ablation. Our imaging data was obtained through 2-photon microscopy of ex-vivo brain slices of transgenic CX3CR1$^{+/GFP}$ mice, which express GFP in microglia and were tail-vein injected with sterile filtered undiluted DyLight 594 labeled Lycopersicon Esculentum (Tomato) Lectin from Vector Labs prior to sacrifice to facilitate targeting of vasculature for microvessel laser ablation to induce microglial response. Before processing, the original data is variance-stabilized to uniform noises and segmented to get the foreground by existing methods [19] [20]. We spent more than 10 hours labeling around 500 tips manually without any help from the proposed method. However, all these tips can be processed within two minutes by our method.

3.2. Experiment and result

We compared our method with four peer methods mentioned before. BS, GC, and SI can also acquire score maps from the data. As with our method, the local maximum of these score maps are regarded as the tips. BS and SI take the average of neighbors to get $d_{\mathbf{p}}^{avg}$ and GC does not to achieve their best performance. RS is more like a decision tree and does not output scores. A detected tip is regarded as a true positive if the nearest distance to ground truth is less than 5 pixels. A real tip in the ground truth can accept one true positive result only.

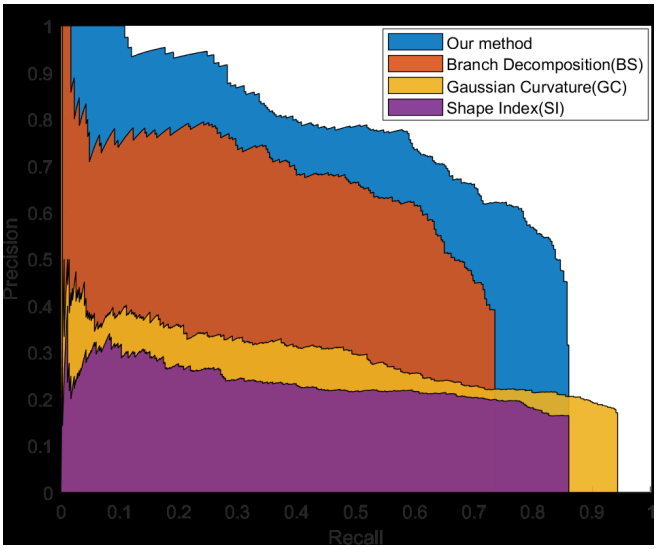

Fig. 2. The precision-recall curves of our method and three peer methods.

We measured the precision and recall of our method and compared to the other three methods with scores. For each method, we set different thresholds to get their precision-recall (PR) curves shown in Fig. 2. We chose PR curves rather than receiver operating characteristic (ROC) curves because PR focuses more on the true positives. The maximum recall may not be up to 100% since results may not include all positive samples. Our method has the best performance of the four methods. The maximum recalls of GC and SI are comparable and even better than our method since the two algorithms detect almost all tiny bumps by utilizing extremely local information, which is also the reason for the low precision. BS is better at detecting sharp tips with small angles but can not handle all tips.

Table 1. Area under curve (AUC) and maximum F-score

	Our	BS	GC	SI	RS
AUC	**0.6879**	0.5081	0.2776	0.2019	N/A
F-score	**0.6843**	0.6123	0.3779	0.3225	0.3837

Table 1 shows the quantitative comparison. Two metrics, the area under curve (AUC) of PR curves and the maximum F-score under different thresholds, are proposed to compare these methods. For RS, AUC is not applicable, and the max-

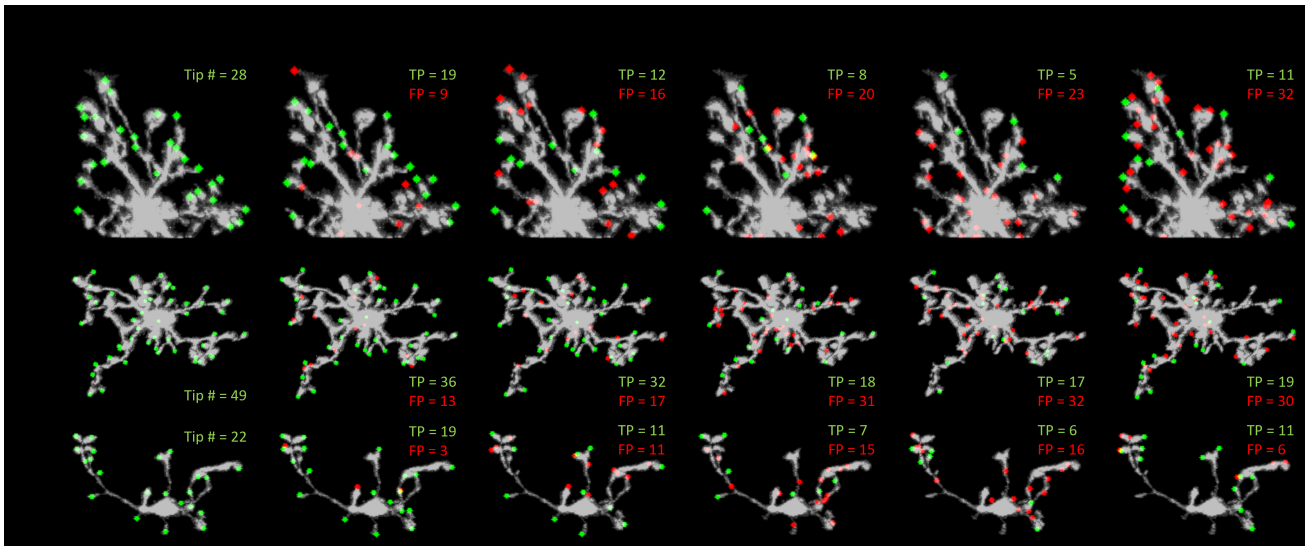

Fig. 3. The detection results of all methods on three cells from our imaging data. Green dots are ground truth or true positives (TP) while red dots are false positives (FP). Cells are segmented from the background and dimmed for better visualization. Every row (a-c) represents one cell. Every column represents one method, where from left to right is: ground truth, our method, branch decomposition, Gaussian curvature, shape index, and ray shooting. For the first four methods, we selected the results with the highest scores whose number is the same as the ground truth. For RS, we can not control the number of results and output all results when achieving the maximum F-score.

imum F-score is from parameter tuning. The performance of BS is much better than other peer methods, but our method has the best performance.

Fig. 3 shows the visualization of detection results. We chose three cells with different morphology. For better visualization, the number of detection results of the first four methods are controlled as the same. As shown in the figure, BS could detect more than half of the tips, but was also influenced by noise and failed to detect tips with certain shapes. GC and SI paid more attention to the irregular surface and ignored the real tip very often. RS was developed for neuron tip detection, which detected tips in 2D stacks firstly and then combined the results in 3D. It may not be applicable to our scene with more complicated patterns. Our method has the most number of true positives and the least number of false positives. However, it may also fail to detect some tips, especially when two tips are merged.

4. CONCLUSION

This paper proposed a novel tip detection approach, which aims at detecting microglia tips in volumetric fluorescence imaging data. The key idea is to measure the distance between the candidate tip and the convex hull of adjacent pixels. Compared to analyzing local patterns, the multi-scale distance metric is more robust to microglia size change and morphology variation.

We compared our approach to four existing methods and did experiments on our in-house data. The precision and recall of results under different score thresholds are exhibited as PR curves. Two metrics, AUC and maximum F-score, were proposed to quantify the results. A part of the detection results of all methods are also visualized with the label of true positives and false positives. Our method has the best performance under all metrics and also has the best visual appearance.

5. COMPLIANCE WITH ETHICAL STANDARDS

All procedures were approved by the USUHS Institutional Animal Care and Use Committee and results are presented according to ARRIVE guidelines. Sample sizes for each experiment were based on previous experience and results from similarly applied techniques in published research. Environmental variables are as regulated by the Department of Laboratory Animal Medicine at USUHS and follow AAALAC guidelines.

6. ACKNOWLEDGEMENTS

Research reported in this publication was partially supported by NIH R01MH110504, NIH U19NS123719 and NSF 1750931. The views expressed in this scientific presentation are those of the authors and do not reflect the official policy or position of the Uniformed Services University, the U.S. government or the Department of Defense.

7. REFERENCES

[1] Florent Ginhoux, Shawn Lim, Guillaume Hoeffel, Donovan Low, and Tara Huber, "Origin and differentiation of microglia," *Frontiers in cellular neuroscience*, vol. 7, pp. 45, 2013.

[2] Anthony J Filiano, Sachin P Gadani, and Jonathan Kipnis, "Interactions of innate and adaptive immunity in brain development and function," *Brain research*, vol. 1617, pp. 18–27, 2015.

[3] Jochen Gehrmann, Yoh Matsumoto, and Georg W Kreutzberg, "Microglia: intrinsic immuneffector cell of the brain," *Brain research reviews*, vol. 20, no. 3, pp. 269–287, 1995.

[4] S Heindl, B Gesierich, C Benakis, G Llovera, M Duering, and A Liesz, "Automated morphological analysis of microglia after stroke. front cell neurosci 12: 106," 2018.

[5] Mahmoud Abdolhoseini, Murielle G Kluge, Frederick R Walker, and Sarah J Johnson, "Segmentation, tracing, and quantification of microglial cells from 3d image stacks," *Scientific reports*, vol. 9, no. 1, pp. 1–10, 2019.

[6] Qingyun Li, Zuolin Cheng, Lu Zhou, Spyros Darmanis, Norma F Neff, Jennifer Okamoto, Gunsagar Gulati, Mariko L Bennett, Lu O Sun, Laura E Clarke, et al., "Developmental heterogeneity of microglia and brain myeloid cells revealed by deep single-cell rna sequencing," *Neuron*, vol. 101, no. 2, pp. 207–223, 2019.

[7] Igor Zingman, Nina Zippel, Gerald Birk, Sebastian Eder, Leo Thomas, Tanja Schönberger, Birgit Stierstorfer, and Fabian Heinemann, "Deep learning–based detection of endothelial tip cells in the oxygen-induced retinopathy model," *Toxicologic Pathology*, vol. 49, no. 4, pp. 862–871, 2021.

[8] Yinghui Tan, Min Liu, Weixun Chen, Xueping Wang, Hanchuan Peng, and Yaonan Wang, "Deepbranch: Deep neural networks for branch point detection in biomedical images," *IEEE transactions on medical imaging*, vol. 39, no. 4, pp. 1195–1205, 2019.

[9] Min Liu, Rong Gong, Weixun Chen, and Hanchuan Peng, "3d neuron tip detection in volumetric microscopy images using an adaptive ray-shooting model," *Pattern Recognition*, vol. 75, pp. 263–271, 2018.

[10] Wei Ma, Bo Xiang, Xiaopeng Zhang, and Hongbin Zha, "Decomposition of branching volume data by tip detection," in *2008 15th IEEE International Conference on Image Processing*. IEEE, 2008, pp. 1948–1951.

[11] Ye Li, YingHui Wang, BingBo Wang, and LianSheng Sui, "Nose tip detection on three-dimensional faces using pose-invariant differential surface features," *IET Computer Vision*, vol. 9, no. 1, pp. 75–84, 2015.

[12] Xiaochen He and Nelson Hon Ching Yung, "Corner detector based on global and local curvature properties," *Optical engineering*, vol. 47, no. 5, pp. 057008, 2008.

[13] Pankaj Kumar, Chunyuan Huang, Jinhai Cai, and Stanley J Miklavcic, "Root phenotyping by root tip detection and classification through statistical learning," *Plant and soil*, vol. 380, no. 1, pp. 193–209, 2014.

[14] Harry Blum et al., *A transformation for extracting new descriptors of shape*, vol. 43, MIT press Cambridge, MA, 1967.

[15] Mattia Montanari and Nik Petrinic, "Opengjk for c, c# and matlab: Reliable solutions to distance queries between convex bodies in three-dimensional space," *SoftwareX*, vol. 7, pp. 352–355, 2018.

[16] Elmer G Gilbert, Daniel W Johnson, and S Sathiya Keerthi, "A fast procedure for computing the distance between complex objects in three-dimensional space," *IEEE Journal on Robotics and Automation*, vol. 4, no. 2, pp. 193–203, 1988.

[17] Stephen Cameron, "Enhancing gjk: Computing minimum and penetration distances between convex polyhedra," in *Proceedings of international conference on robotics and automation*. IEEE, 1997, vol. 4, pp. 3112–3117.

[18] Sawsen Abdulhadi Mahmood, Rana Fareed Ghani, and Abdulamir Abdullah Kerim, "Nose tip detection using shape index and energy effective for 3d face recognition," *Int. J. Mod. Eng. Res.(IJMER)*, vol. 3, no. 5, pp. 3086–3090, 2013.

[19] Mengfan Wang, Boyu Lyu, and Guoqiang Yu, "Convexvst: A convex optimization approach to variance-stabilizing transformation," in *International Conference on Machine Learning*. PMLR, 2021, pp. 10839–10848.

[20] Yizhi Wang, Congchao Wang, Petter Ranefall, Gerard Joey Broussard, Yinxue Wang, Guilai Shi, Boyu Lyu, Chiung-Ting Wu, Yue Wang, Lin Tian, et al., "Synquant: an automatic tool to quantify synapses from microscopy images," *Bioinformatics*, vol. 36, no. 5, pp. 1599–1606, 2020.